Engineering Geology 207 (2016) 103–114

Contents lists available at ScienceDirect

Engineering Geology

journal homepage: www.elsevier.com/locate/enggeo

Three-dimensional hydrogeological reconstruction based on geological depositional model: A case study from the coastal plain of Arborea (Sardinia, Italy)

Giorgio Ghiglieri [a,b,*], Alberto Carletti [a,b], Stefania Da Pelo [a], Fabrizio Cocco [a], Antonio Funedda [a], Alfredo Loi [a], Fabio Manta [a], Daniele Pittalis [b,c]

[a] Department of Chemical and Geological Sciences, University of Cagliari, Via Trentino 51, 09127 Cagliari, Italy
[b] Desertification Research Centre (NRD), University of Sassari, Viale Italia, 07100 Sassari, Italy
[c] Department of Physics and Earth Sciences, University of Parma, Parco Area delle Scienze 157a, 43124 Parma, Italy

ARTICLE INFO

Article history:
Received 13 October 2015
Received in revised form 4 April 2016
Accepted 15 April 2016
Available online 19 April 2016

Keywords:
3D hydrogeological–conceptual model
Groundwater
Nitrate pollution
Nitrate Vulnerable Zone
Desertification
Sardinia

ABSTRACT

This study presents a novel approach for the hydrogeological assessment of sedimentary coastal aquifers. Specifically, the methodology is tailored for modeling groundwater flow and nitrates contamination in typical Mediterranean coastal plains with high anthropogenic pressures, as exemplified by the Arborea plain (central western Sardinia, Italy). The study started with development of an updated geological–depositional model based on sequential stratigraphy. Geological and geophysical data, processed in a geographic information system (GIS) environment, supported the definition of a 3D hydrogeological conceptual model and provided a solid basis for the interpretation of groundwater flow directions. The 3D hydrogeological model allowed constraining groundwater circulation, flow paths and distribution of nitrate concentrations in the aquifers. The methodology appears as a valid tool applicable in other coastal areas to determine geological and hydrogeological settings. The definition of a quantitative hydrogeological framework will support the effective management of local water resources.

© 2016 Elsevier B.V. All rights reserved.

1. Introduction

The contamination by nitrate (NO_3^-) of groundwater is becoming a ubiquitous problem. The World Health Organization has recommended a threshold of 50 mg L^{-1} in drinking water (WHO, 2003), but groundwater concentrations in Europe commonly exceed this level in 22% of cultivated land (Sacco et al., 2007), and similar concentrations occur in arable areas of the USA (Canter, 1997). The concern about the potential pollution of groundwater because of increasing human pressure on the environment has led to the development of an extensive legal framework. Both the 91/676 and 2006/118 Directives, issued by European Commission respectively for the protection of waters from nitrates of agricultural origin and for the protection of groundwater against pollution and deterioration (Groundwater Directive — GWD), have been implemented in Italy. Nitrates Directive states that all areas of land which drain into waters exceeding the concentration of 50 mg L^{-1} of NO_3 and which contribute to nitrate pollution must be designated as "Nitrate Vulnerable Zones" (NVZs). In these areas, farmers are required to comply with specific measures directed to improve water quality. Although the Directive clearly states the criteria for identifying NVZs, the implementation of these criteria has varied from country to country. The designation of an NVZ must take into account all relevant physical and environmental factors (i.e. aquifer characteristics, flows and solute transport in the saturated zone, the behavior of nitrogen compounds in the environment and land use) that may influence the nitrogen dynamics.

Many NVZs worldwide are located in flat lands and in coastal areas where the intense agricultural activity, the high concentration of inhabitants and the seasonal population determine a significant water demand. In those areas, several environmental concerns may occur at the same time. Indeed, in farmed coastal zones the impacts on water resources include pollution due to nutrient and pesticide leaching and seawater intrusion into aquifers (Steinich et al., 1998; Zalidis et al., 2002; Ghiglieri et al., 2012). Groundwater management in coastal aquifers requires the elaboration of a local geological and hydrogeological conceptual model in order to understand the processes determining the quality of water, the hydrodynamic parameters and the productivity of aquifers.

During the last few years, techniques in 3D hydrogeological model reconstruction/visualization have been improved (Wu et al., 2005; Jones et al., 2009; Wycisk et al., 2009; Best and Lewis, 2010; Cox et al.,

* Corresponding author at: Department of Chemical and Geological Sciences, University of Cagliari, Via Trentino 51, 09127 Cagliari, Italy.
E-mail addresses: ghiglieri@unica.it (G. Ghiglieri), acarletti@uniss.it (A. Carletti), sdapelo@unica.it (S. Da Pelo), fabrcocco@gmail.com (F. Cocco), afunedda@unica.it (A. Funedda), alfloi@unica.it (A. Loi), fabio.mantax@gmail.com (F. Manta), daniele.pittalis@unipr.it (D. Pittalis).

http://dx.doi.org/10.1016/j.enggeo.2016.04.014
0013-7952/© 2016 Elsevier B.V. All rights reserved.

2013; Di Maio et al., 2014) by integrating different sets of data (e.g. geological, hydrogeological, geophysical). The 3D geological approach is routinely used in mineral deposits or hydrocarbon reservoir assessment (Jones et al., 2009). By contrast, for the hydrogeological studies and hydrogeochemical characterization of groundwater this approach is not yet routinely used (Raiber et al., 2012). Different methodologies to develop 3D geological models have been elaborated and tested (Lemon and Jones, 2003; Smirnoff et al., 2008; Tremblay et al., 2010). However, currently there are no perfect methods or a comprehensive modeling approach for the reconstruction of sedimentary stratigraphic systems. According to the international literature, one of the main problems is the discontinuous spatial distribution of stratigraphical information, mainly due to the lack of borehole data that can lead to an inaccurate 3D geological conceptual model.

The geology in coastal areas is complex because of the large number of interacting terrestrial and marine processes. Groundwater flow and travel time depend on stratigraphic setting which controls boundary conditions of the aquifers (Edington and Poeter, 2006). Moreover, in such environments sediment stacking (sand, gravel, clay) is typically repeated many times, allowing for a variety of possible correlations. Therefore, it is not straightforward to reconstruct a realistic geological model.

In order to correlate the sedimentary facies in a reliable and meaningful way, sequence stratigraphy, which describes succession through space and time in various depositional systems (Dalrymple and Choi, 2007), has been employed. For this purpose, the definition of the hydrogeological framework, obtained by integrating geological, stratigraphic and hydrogeological data, represented the basis for predicting groundwater circulation and pollutant diffusion (Di Salvo et al., 2012; Irace et al., 2010). The management of water resources is central to any attempt to conserve both water quality and quantity (Ghiglieri et al., 2009a,b).

The aim of the research was to develop a methodology suitable for sedimentary coastal aquifers for compiling quantitative hydrogeological information. The study was carried out within the framework of the interdisciplinary IDRISK (*Pollution risk and prevention of groundwater degradation*) and KNOW (implementing the Knowledge of NitrOgen in groundWater) Projects (http://nrd.uniss.it). It had the twin goal of elaborating a local hydrogeological conceptual model and defining the major groundwater flows, in order to predict the diffusion of NO_3^- in the aquifers.

To achieve these objectives, it was necessary to refine the depositional-geological model of the sedimentary basin underlying the Arborea plain (located on the West cost of Sardinia, Italy). The study then started with a geological characterization of the study area, based on a set of data arising from stratigraphic log wells and vertical electrical soundings (VESs). The data (stratigraphic, geological, hydrogeological and geochemical) were implemented in a Geographic Information System (GIS) and in a conceptual Data Base (DB). This DB was interfaced with several softwares e.g. Move (Midland Valley Exploration), to build a 3D hydrogeological model. A calibration and validation of the hydrogeological framework was obtained from measured NO_3^- concentrations in groundwater samples.

2. Description of the study area

The study area is located in the northern part of the Campidano plain (central-western Sardinia, Italy: Fig. 1a). It is limited to the north and to the east respectively by the volcanic complexes of Montiferru and Monte Arci, to the south by the Mogoro River, Marceddì and San Giovanni lagoons and by the sea of the Oristano Gulf to the west. The Tirso River, the most important river in Sardinia, crosses the northern part of the plain and flows in a SW direction towards the Oristano Gulf. The Arborea plain covers about 60 km^2 portion of the area, lying between the coast and the reclaimed Sassu lagoon (Fig. 1b). It was reclaimed during the 1920s for agricultural purposes and has been used to produce irrigated crops ever since. It remains one of the most productive agricultural locations on the island, achieving a level of dairy productivity among the highest in Italy. Double cropping of silage maize and Italian ryegrass is practiced on more than 80% of the irrigated area, and the biomass is used to feed about 35,000 dairy cattle raised in intensive systems (Giola et al., 2012); the remaining land is used to grow lucerne and various horticultural crops (Foddis et al., 2012).

2.1. Geological setting

Following the collision between the South European Plate and the Adria Plate during the early Miocene, Sardinia separated from the European continent during the Lower-Middle Miocene (Carmignani et al., 2001; Oggiano et al., 2009). During these major geodynamic events, several basins formed on the island, particularly on its western side. Volcano-sedimentary materials filled the basins aligned in a NNW–SSE direction and bounded by normal faults. During the Plio-Pleistocene, a new extensional phase associated with the South Tyrrhenian opening reactivated a series of NNW–SSE fault lines. Consequently the Campidano trough developed. The general subsidence associated with this extension, combined with climatic oscillations and regressive and transgressive marine variations, produced a landscape characterized by thick sedimentary layers of littoral-marine and fluvial-deltaic material. Seismic surveys and geological logs, conducted in the Campidano plain since the 1960s, provided information on the current state of the local stratigraphy and the geological structure at depth (Casula et al., 2001; Cocco et al., 2013). The Oristanese area is a half-graben bounded by faults arranged in N–S direction, which contributed to a deepening of the basin on its western edge, where the Sinis main fault lies. This structure, easily recognized in seismic cross-sections, was certainly active after the deposition of the basaltic-lava flows in early Pleistocene times (Cocco et al., 2013). In the Arborea plain, the sedimentary succession that fills the Campidano trough is up to 1000 m in thickness and overlies the Miocene volcano-sedimentary succession. During the Quaternary, the deposition of continental and coastal marine sediments related to the Quaternary glacioeustatic cycles affected the littoral and low-lying areas (Lecca and Carboni, 2007). Structural and morphological factors determined the thickness of these deposits, generally arranged in a highstand system geometry (Buttau et al., 2011).

3. Materials and methods

3.1. Stratigraphic analysis, geological cross sections and 3D hydrogeological model

Fig. 2 reports the conceptual workflow of the methodological approach. The stratigraphic analysis was based on a set of both surface and sub-surface observations.

The geological features of the study area were inferred by the official 1:25,000 map of Sardinia, available in digital form at www.sardegnageoportale.it. The stratigraphic data were gathered from 143 wells, provided by Sardinia Regional Agencies (ARPAS, LAORE) or available from previous projects (CASMEZ, 1976) and from unpublished work (Fig. 1b).

A set of 96 VESs (Casmez, 1976) evenly distributed across the study area was an important source of additional data (Fig. 1b). The resulting apparent resistivity curves of each VES were interpreted by a computer program, based on the linear digital filtering method (Koefoed, 1972, 1979; O'Neill and Merrick, 1984). Current software packages based on this approach are able to cope with extreme apparent resistivity contrasts and to deal with a large number of layers. The association of a specific lithology with a given resistivity value took into account the stratigraphic log of wells located close to each VES.

A GIS database was populated with the position, elevation, depth, characterization of litho-stratigraphic layering and the top and bottom surface elevations for each well and VES. An ArcGis tool (ArcGis eXacto

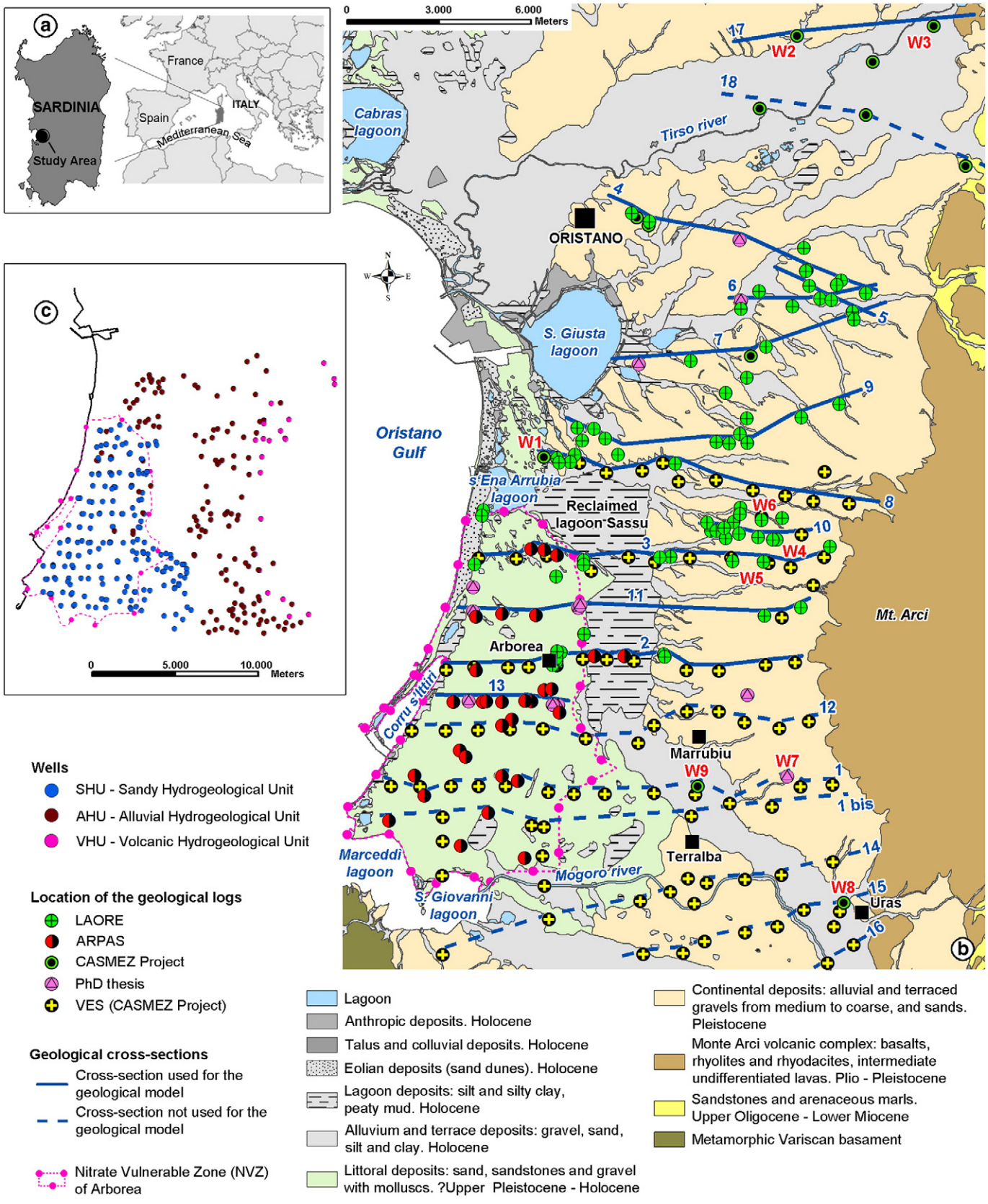

Fig. 1. Geographical map of the study area; b) geological cross-sections, stratigraphic log wells and VES locations; c) locations of wells for the hydrogeological survey.

Section v2.0), developed by the Illinois State Geological Survey, processed each geological cross-section, which was then finalized by a graphic software. The software package Move (www.mve.com/software/move) was used to verify the three dimensional consistency of the geological model. As a first step, several geological sections were elaborated. Based on the number of stratigraphic logs and VESs

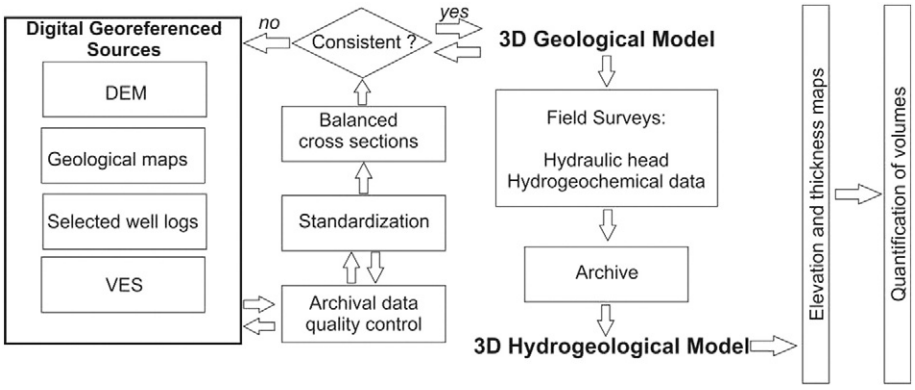

Fig. 2. Flowchart for methodology of 3D hydrogeological model building.

available for their validation, twelve sections were considered of good quality and used for the reconstruction of the geological model (Fig. 1b).

According to the conceptual hydrogeological model described below (Section 4.2), the 3D hydrogeological model identified three main surfaces. These surfaces matched the base of the Alluvial Hydrogeological Unit (AHU), the top of the Alluvial Hydrogeological Unit (AHU) and the base of the Sandy Hydrogeological Unit (SHU).

Every surface was modeled by interpolation of the contour lines (depths) drawn taking into account the geological cross-sections, the well data and the interpreted VES data. To the south of the Sassu lagoon, where the reconstruction of the geological cross-sections was not possible due to the small number of stratigraphic logs available, the contour lines were drawn based on the surface geology and following the trend of the contour lines modeled in the northern sector of the Arborea plain.

3.2. Hydrogeological and geochemical data

Two field surveys were carried out during 2011. In the first one, 354 wells were investigated between March and May (Fig. 1c). At each well, elevation and geographical coordinates (using a differential global positioning system), constructive and technical data of each well and piezometric level were acquired. Groundwater electrical conductivity, pH and temperature were analyzed in situ, using a portable multiparameter probe (WTW pH-cond 340i). During the second survey, carried out in September 2011, measures of piezometric level, pH, electrical conductivity and temperature were repeated. Groundwater were also collected from the well pump outflow for NO_3^- analysis, and stored under cool conditions in 100 mL polyethylene bottles until assayed using an ion-selective electrode mounted on an ORION 5 STAR device. For each water point, the data were inserted into a digital database and GIS, using ArcGIS v10.0.

4. Results

Table 1 reports the list of the more representative geological logs (wells) employed to reconstruct the geological sections.

On the basis of stratigraphic log interpretation, Quaternary succession is represented by an alternation of generally loose fine and coarse sand, with occasional and discontinuous layers of clay. In some wells (W2 through W7), the Quaternary sequences overlie a basement of volcanic rocks belonging to the Plio-Pleistocene Monte Arci complex (Fig. 1b). At the margin of the basin, the thickness of the sedimentary succession varies from 40 m (W7) to 132 m (W6). The wells in the central part of the plain were drilled to a depth of 200 m, but did not reached the volcanic basement. Only W1 (1800 m) completely penetrated the Plio-Quaternary sedimentary succession (Pomesano-Cherchi, 1971), reaching the underlying volcanic rock at a depth of 304 m. The inference is that the basin deepens progressively from east to west.

The sediments identified in the wells and outcrops in the Arborea and Oristano plains belong to established classes of Quaternary deposits, namely:

- alluvial sediments, formed by sand with some silt and clay, which give way quickly (especially in the Tirso River area) to medium to coarse gravel, more or less clayey (Holocene);
- lagoonal deposits, consisting of silt and clay (Holocene);

Table 1
Stratigraphic log wells and VES resistivity logs used to construct the geological model.

ID_COD	Denomination	Location	Data source	Elevation	Depth
W1	OR_1	Sassu	CASMEZ	4	1802.0
W2	P3 casmez	Solarussa	CASMEZ	10	32.0
W3	P4 casmez	Ollastra Simaxis	CASMEZ	9	98.0
W4	P2 217 III NE	Marrubiu	LAORE	42	186.5
W5	P3 217 III NE	Marrubiu	LAORE	39	176.5
W6	P4 217 III NE	Marrubiu	LAORE	30	190.0
W7	GC78	Terralba	PhD Thesis	33	96.0
W8	P7 casmez	Uras	CASMEZ	16	82.0
W9	P22 casmez	Marrubiu	CASMEZ	7	96.0
W10	P3 217 III NO	Arborea	LAORE	2	30.0
W11	F1	Capo della Frasca	VES	2	64.0
W12	F2	Capo della Frasca	VES	6	758.0
W13	P20	Strada 27 ovest (Arborea)	ARPAS	6	7.4
W15	G14	Arborea	VES	5	260.0
W16	P26	Strada 26 est. (Arborea)	ARPAS	4	16.5
W17	P37 217 III NE	Arborea	LAORE	5	50.0
W18	P26 217 III NE	Arborea	LAORE	4	35.8
W19	G16	Arborea	VES	1	189.0
W20	G17	Arborea	VES	2	376.0
W21	P41 217 III NE	Arborea	LAORE	5	50.0
W22	P36 217 III NE	Arborea	LAORE	8	200.0
W23	G18	Arborea	VES	12	509.0
W24	G19	Arborea	VES	24	605.0
W25	P8 217 III NE	Marrubiu	LAORE	24	143.0
W26	G20	Arborea	VES	42	186.0
W27	G21	Arborea	VES	55	551.0
W28	G23	Arborea	VES	93	231.0
W29	P16 217 III NE	Santa Giusta	LAORE	4	86.0
W30	P19 217 III NE	Santa Giusta	LAORE	4	0.0
W31	P17 217 III NE	Santa Giusta	LAORE	1	140.0
W32	G1	Arborea	VES	2	197.0
W33	G2	Arborea	VES	−1	773.0
W34	G3	Arborea	VES	1	73.0
W36	P27 217 III NE	Santa Giusta	LAORE	11	100.0
W37	G6	Arborea	VES	14	159.0
W38	G7	Arborea	VES	25	742.0
W39	G8	Arborea	VES	39	60.0
W40	G9	Arborea	VES	48	779.0
W41	G11	Arborea	VES	74	330.0

Elevation is in m a.s.l.; depth is in m.

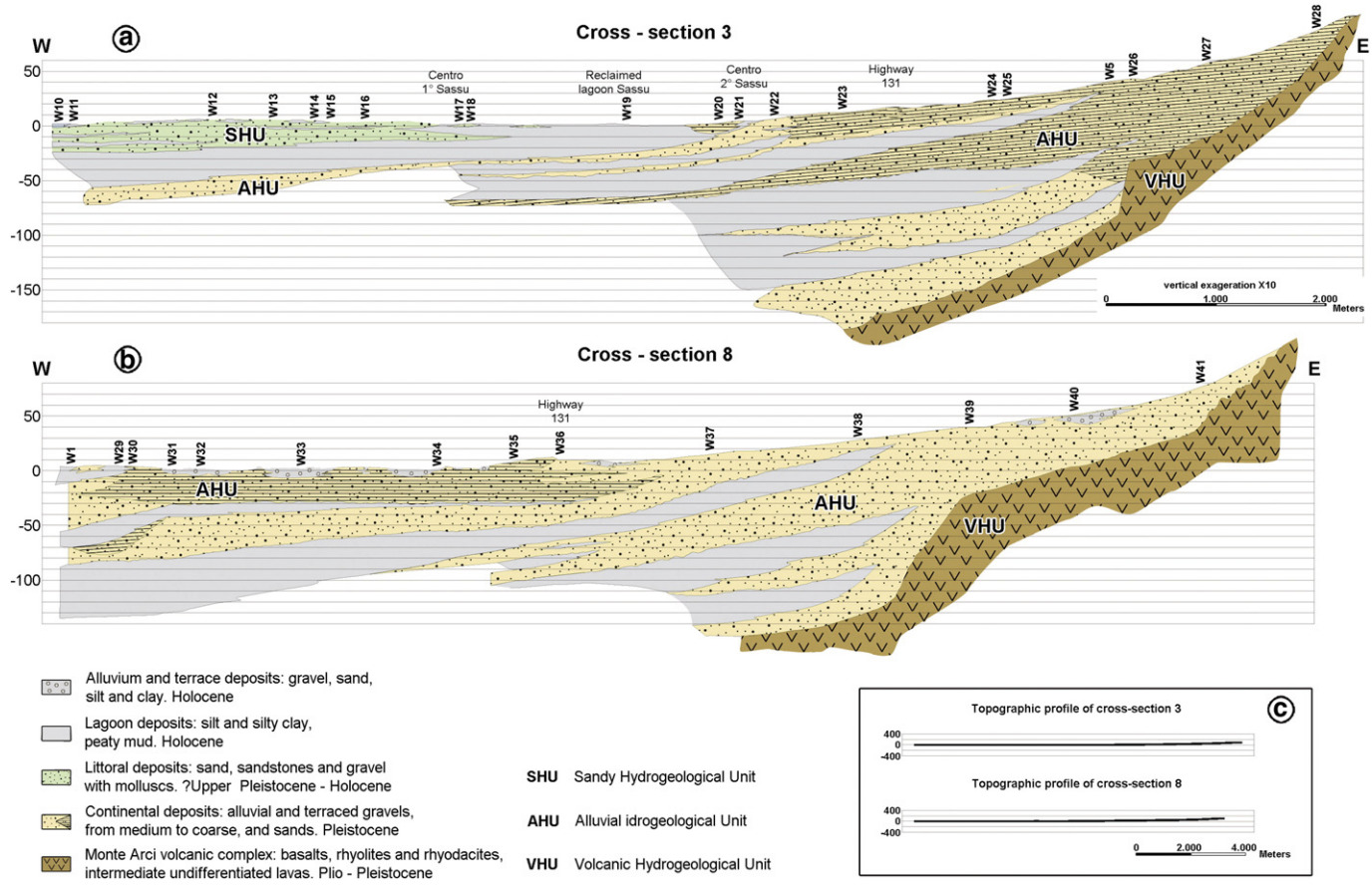

Fig. 3. Geological cross-sections: a) cross-section #3; b) cross-section #8; c) topographic profiles of the cross-sections.

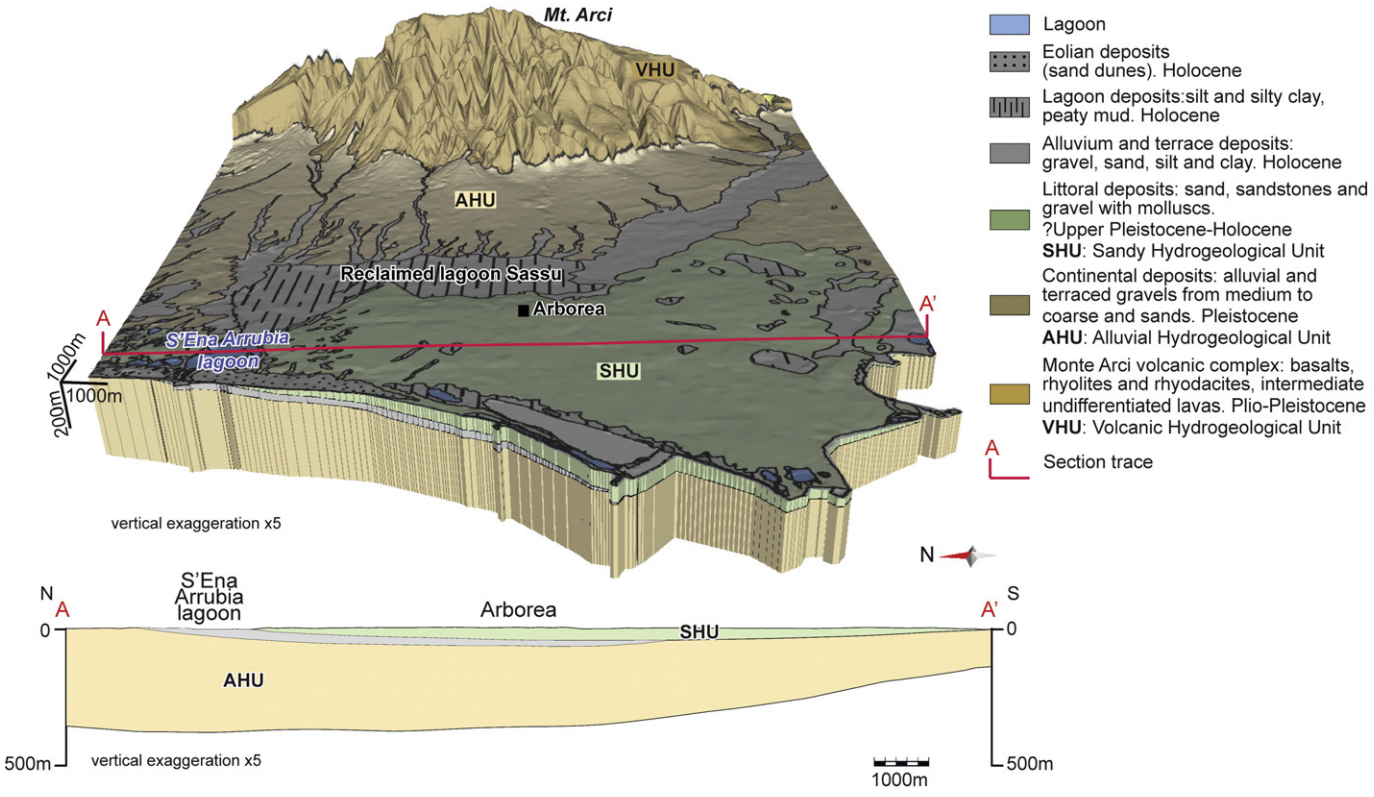

Fig. 4. 3D hydrogeological model.

Table 2
Piezometric head of the well monitoring network and NO_3 concentrations of the groundwater sampled in the September 2011 survey.

ID	HU	Depth	Piez. head	NO_3	ID	HU	Depth	Piez. head	NO_3	ID	HU	Depth	Piez. head	NO_3	ID	HU	Depth	Piez. head	NO_3
P1	AHU	5.00	−0.14*	**204.50**	P50	SHU	22.00	−1.08*	8.24	P99	SHU	3.00	2.21	**104.00**	P148	VHU	126.00	n.a.	5.42
P2	AHU	53.00	0.15*	34.90	P51	SHU	2.36	3.50	23.00	P100	SHU	18.00	1.12*	4.89	P149	AHU	60.00	15.39*	8.04
P3	SHU	7.00	0.46*	**287.00**	P52	SHU	23.00	−0.48*	**146.00**	P101	SHU	2.60	2.17	43.80	P150	AHU	60.00	15.92*	n.a.
P4	SHU	24.00	−0.05*	32.50	P53	SHU	3.60	3.84	12.30	P102	SHU	2.60	0.15*	**107.00**	P151	AHU	20.00	20.76*	**107.50**
P5	SHU	4.00	1.50*	**92.90**	P54	SHU	27.00	0.41*	**80.00**	P103	SHU	20.00	1.59*	**73.40**	P152	AHU	80.00	7.22	n.a.
P6	SHU	19.00	0.44*	2.95	P55	SHU	35.00	−0.48*	9.00	P104	SHU	3.00	2.75	17.75	P153	VHU	105.00	n.a.	4.68
P7	AHU	80.00	0.43*	11.60	P56	SHU	30.00	−0.44*	8.27	P105	SHU	33.00	0.71*	9.75	P154	VHU	150.00	n.a.	n.a.
P8	SHU	14.00	0.26*	27.25	P57	SHU	33.00	−0.71*	9.64	P106	SHU	37.00	0.77	28.30	P155	VHU	125.00	32.36	n.a.
P9	SHU	21.00	0.26	37.90	P58	SHU	2.65	1.84	10.90	P107	SHU	24.00	n.a.	**102.00**	P156	VHU	110.00	n.a.	15.60
P10	SHU	27.00	n.a.	4.93	P59	SHU	22.00	−0.33*	11.20	P108	SHU	40.00	0.68*	37.45	P157	AHU	90.00	n.a.	0.00
P11	SHU	3.30	3.23	4.72	P60	SHU	25.00	−2.51*	11.00	P109	SHU	21.00	0.54*	34.40	P158	AHU	n.a.	25.75	n.a.
P12	SHU	5.70	2.89	**80.70**	P61	SHU	4.25	5.35	11.50	P110	SHU	30.00	−0.74*	18.00	P159	VHU	60.00	23.32*	17.10
P13	SHU	22.00	−0.27*	**234.50**	P62	AHU	80.00	−2.56*	21.60	P111	SHU	15.00	1.37*	10.40	P160	VHU	77.00	23.98*	**56.50**
P14	SHU	5.00	1.18*	9.75	P63	SHU	50.00	0.43*	21.00	P112	SHU	14.00	0.16*	26.80	P161	VHU	80.00	16.40*	33.90
P15	SHU	23.00	0.49	33.10	P64	SHU	40.00	−2.09*	5.20	P113	SHU	13.00	1.23*	**108.00**	P162	AHU	8.50	26.18	6.64
P16	SHU	3.30	3.73	**84.80**	P65	SHU	22.00	−0.65*	6.73	P114	SHU	19.00	1.24*	**123.00**	P163	VHU	60.00	16.91	49.50
P17	SHU	31.00	1.41*	5.34	P66	SHU	2.40	2.07	19.90	P115	SHU	3.70	1.51	22.70	P164	AHU	3.70	29.15	2.65
P18	SHU	15.00	0.49	6.40	P67	SHU	20.00	0.29	10.20	P116	SHU	27.00	−1.03*	**121.00**	P165	AHU	50.00	16.30*	**76.50**
P19	SHU	3.00	1.91	**104.00**	P68	SHU	50.00	−0.19*	10.60	P117	SHU	19.00	1.12*	**110.00**	P166	VHU	60.00	15.65	11.90
P20	SHU	38.00	0.46	n.a.	P69	SHU	3.50	n.a.	n.a.	P118	SHU	20.00	1.99*	**233.50**	P167	VHU	105.00	23.20*	12.90
P21	AHU	99.00	0.37*	29.95	P70	SHU	22.00	0.59*	6.35	P119	SHU	4.50	4.80	35.70	P168	AHU	13.00	15.08*	33.40
P22	SHU	23.00	−0.94*	5.07	P71	SHU	32.00	−1.86*	11.60	P120	SHU	14.00	1.36*	**165.00**	P169	AHU	12.00	13.82*	46.80
P23	AHU	60.00	0.00*	23.30	P72	SHU	22.00	−3.54*	15.90	P121	SHU	20.00	0.41*	**70.60**	P170	AHU	8.60	11.81*	**102.50**
P24	SHU	2.80	3.93	8.35	P73	SHU	25.00	0.23*	14.55	P122	SHU	25.00	1.67*	**186.00**	P171	AHU	8.70	12.36	**130.50**
P25	SHU	23.00	0.32*	15.55	P74	SHU	2.40	2.70	**73.10**	P123	SHU	9.00	1.98*	**161.50**	P172	AHU	8.00	12.09	**52.40**
P26	SHU	4.65	1.55*	5.43	P75	SHU	46.00	−2.35*	14.15	P124	SHU	22.00	1.02*	**166.00**	P173	AHU	3.40	9.68	36.85
P27	SHU	24.00	1.27*	9.95	P76	SHU	31.00	0.79*	32.40	P125	SHU	12.00	0.07*	17.60	P174	AHU	5.50	12.12	11.70
P28	SHU	15.00	−4.36*	10.80	P77	SHU	3.90	6.18*	**272.00**	P126	SHU	30.00	0.69	16.80	P175	AHU	6.00	13.67	**71.50**
P29	AHU	74.00	−1.07	11.40	P78	SHU	18.00	n.a.	31.70	P127	SHU	2.40	0.74	20.10	P176	AHU	5.50	10.04	**105.00**
P30	SHU	6.25	5.11*	**130.00**	P79	SHU	25.00	0.77*	**103.00**	P128	SHU	18.00	1.39*	**104.00**	P177	VHU	55.00	17.66*	9.37
P31	SHU	12.00	3.44	**58.70**	P80	SHU	15.00	0.16*	8.86	P129	SHU	3.00	0.33*	**105.00**	P178	AHU	30.00	20.47	22.80
P32	SHU	25.00	0.09*	5.55	P81	SHU	40.00	−0.18*	35.75	P130	SHU	27.00	0.73*	29.40	P179	AHU	6.00	14.11	**55.00**
P33	SHU	4.50	3.91*	10.90	P82	SHU	2.00	2.50	18.90	P131	SHU	18.00	1.74	**173.00**	P180	AHU	5.00	12.75	**64.00**
P34	SHU	30.00	2.45	**135.00**	P83	SHU	45.00	0.35*	30.10	P132	SHU	7.00	1.33*	**260.00**	P181	AHU	4.00	10.99	**98.00**
P35	AHU	68.00	−1.09	**162.50**	P84	SHU	30.00	0.75	6.13	P133	SHU	29.00	0.62*	15.20	P182	AHU	7.00	10.21	**58.00**
P36	SHU	4.00	5.21	1.65	P85	AHU	100.00	n.a.	9.00	P134	SHU	2.50	1.21*	**251.00**	P183	AHU	5.00	13.48	**85.30**
P37	SHU	21.00	1.04*	36.50	P86	AHU	50.00	−4.19	11.40	P135	VHU	100.00	21.35	3.24	P184	AHU	33.00	20.82*	**105.50**
P38	SHU	22.00	0.38*	4.06	P87	SHU	25.00	0.94*	26.30	P136	VHU	98.00	22.33*	21.80	P185	SHU	16.00	0.08*	0.00
P39	SHU	18.00	−0.25*	**85.00**	P88	SHU	5.60	1.02*	**65.00**	P137	AHU	n.a.	21.01	8.58	P200	SHU	60.00	−2.64*	6.26
P40	SHU	2.60	2.82	**149.00**	P89	SHU	27.00	0.99*	**52.00**	P138	VHU	102.00	22.45	35.50	P201	SHU	18.00	−5.85*	6.58
P41	SHU	46.00	0.41	**159.00**	P90	SHU	3.70	3.06	7.45	P139	VHU	80.00	20.61	21.00	P202	SHU	7.00	5.04	23.00
P42	SHU	15.00	−0.07*	**83.00**	P91	SHU	28.00	0.89*	21.00	P140	VHU	130.00	n.a.	n.a.	P203	SHU	8.00	4.50	16.40
P43	SHU	2.30	−0.06	n.a.	P92	SHU	50.00	−0.61*	16.00	P141	AHU	4.00	52.55	16.60	P204	SHU	25.00	−1.95*	5.72
P44	SHU	15.00	2.37*	**114.50**	P93	SHU	2.20	1.88	**89.90**	P142	VHU	108.00	20.66*	6.95	P205	SHU	3.00	4.02*	**169.00**
P45	SHU	19.00	−0.99*	47.65	P94	SHU	17.00	0.72*	37.85	P143	VHU	70.00	20.99*	10.90	P206	AHU	42.00	−6.50*	8.44
P46	SHU	18.00	0.47*	**115.00**	P95	SHU	85.00	−1.17*	12.60	P144	VHU	74.00	9.87*	13.00	P207	SHU	12.00	0.95*	**187.00**
P47	SHU	7.00	−0.80*	33.40	P96	SHU	2.40	2.25	**141.00**	P145	VHU	n.a.	n.a.	n.a.	P208	SHU	18.00	−0.51*	3.48
P48	SHU	2.30	1.22*	**195.50**	P97	SHU	47.00	0.18*	21.95	P146	AHU	40.00	19.08*	18.10	P209	SHU	4.00	4.08	**146.00**
P49	SHU	37.00	−0.37*	7.11	P98	SHU	18.00	0.99*	13.40	P147	AHU	70.00	20.54	2.47	P210	AHU	54.00	n.a.	11.50
P211	AHU	53.00	−2.10*	12.20	P251	AHU	150.00	−0.24	5.88	P291	AHU	4.00	n.a.	n.a.	P331	AHU	20.00	6.63*	29.40
P212	SHU	12.00	2.30	**94.00**	P252	AHU	35.00	−1.28	17.40	P292	AHU	30.00	2.31*	5.72	P332	AHU	140.00	15.47*	**83.20**
P213	SHU	12.00	1.72	**87.30**	P253	AHU	28.00	−0.96*	13.50	P293	AHU	54.00	1.10*	6.47	P333	AHU	5.00	22.25	25.70
P214	SHU	11.00	1.83	**89.90**	P254	SHU	26.00	−0.62	33.45	P294	AHU	6.00	0.12	44.80	P334	AHU	9.00	32.25	43.10
P215	SHU	12.00	1.82*	**213.00**	P255	AHU	40.00	7.72*	31.90	P295	AHU	8.00	0.34	**202.00**	P335	AHU	30.00	n.a.	n.a.
P216	SHU	8.00	2.20*	**195.00**	P256	AHU	60.00	4.45*	34.60	P296	AHU	14.00	0.53*	**197.00**	P336	AHU	30.00	5.22	11.10
P217	SHU	13.00	n.a.	10.70	P257	AHU	85.00	3.71*	4.87	P297	AHU	20.00	0.28	35.10	P337	AHU	30.00	4.22	15.70
P218	SHU	11.00	1.81*	**143.00**	P258	AHU	30.00	2.21*	7.62	P298	AHU	12.00	0.55*	4.30	P338	AHU	7.00	6.83	**53.70**
P219	SHU	52.00	−13.01*	6.92	P259	AHU	40.00	n.a.	7.11	P299	AHU	15.00	0.47*	**145.00**	P339	AHU	7.00	8.49	**70.30**
P220	SHU	22.00	0.22*	**144.00**	P260	AHU	82.00	8.92*	**57.30**	P300	AHU	12.00	0.32	**60.00**	P340	AHU	8.00	9.89	**137.50**
P221	SHU	50.00	−15.87*	7.59	P261	AHU	28.00	−0.84*	5.80	P301	AHU	97.00	2.18*	4.91	P341	AHU	46.00	8.65*	**79.00**
P222	SHU	36.00	−1.41*	14.30	P262	SHU	8.00	−0.82*	**62.50**	P302	AHU	15.00	0.17	**174.00**	P342	AHU	40.00	8.07*	**56.60**
P223	SHU	18.00	−1.18	29.35	P263	AHU	5.00	n.a.	n.a.	P303	AHU	9.00	8.82	**123.00**	P343	AHU	36.00	8.38*	19.00
P224	SHU	3.00	5.60	**59.20**	P264	AHU	25.00	4.94*	**73.50**	P304	AHU	10.00	7.49	**100.00**	P344	AHU	38.00	7.88	**103.50**
P225	SHU	50.00	−4.79*	11.10	P265	AHU	40.00	n.a.	**97.20**	P305	AHU	9.00	7.42	**99.60**	P345	AHU	10.00	4.83	**85.50**
P226	SHU	16.00	−2.10*	29.20	P266	AHU	5.00	1.46	**109.00**	P306	AHU	9.00	6.28	**120.50**	P346	AHU	8.00	6.35	8.97
P227	SHU	24.00	−1.26*	18.65	P267	AHU	14.50	3.69	**77.80**	P307	AHU	8.00	6.84*	**82.90**	P347	AHU	7.00	5.21	**99.60**
P228	AHU	80.00	−1.51*	6.21	P268	AHU	40.00	−31.87*	14.70	P308	AHU	30.00	7.84*	**53.00**	P348	SHU	5.00	4.70	11.60
P229	SHU	3.00	5.81	4.35	P269	AHU	12.00	0.65	9.00	P309	AHU	10.00	8.48	**56.00**	P349	SHU	28.00	1.84*	**107.00**
P230	SHU	28.00	1.01*	21.40	P270	SHU	10.00	1.67	**95.50**	P310	SHU	8.00	2.26	**251.00**	P350	SHU	8.00	4.92	1.58
P231	SHU	24.00	1.66*	44.60	P271	SHU	12.00	1.73*	**61.70**	P311	SHU	27.00	2.59*	**76.30**	P351	SHU	16.00	0.97*	**196.00**
P232	SHU	18.00	1.60*	42.70	P272	SHU	6.00	1.43	**174.50**	P312	SHU	8.00	1.88	**61.00**	P352	SHU	12.00	1.21*	**351.00**
P233	SHU	22.00	1.68*	**57.90**	P273	SHU	4.00	1.35	**94.00**	P313	SHU	8.00	2.93	47.10	P353	SHU	9.00	3.28	**67.60**
P234	SHU	90.00	n.a.	n.a.	P274	SHU	12.00	1.37	**97.70**	P314	SHU	6.00	1.46	16.30	P354	SHU	17.00	4.40*	**196.50**
P235	SHU	26.00	1.89*	**256.00**	P275	SHU	6.00	1.55	9.05	P315	SHU	8.00	2.31	**406.00**	P355	SHU	11.00	3.93	**71.80**
P236	AHU	70.00	−9.19*	**53.90**	P276	SHU	40.00	−6.23*	9.35	P316	SHU	18.00	2.81	48.60	P356	SHU	9.00	1.92	**318.00**

Table 2 (*continued*)

ID	HU	Depth	Piez. head	NO_3	ID	HU	Depth	Piez. head	NO_3	ID	HU	Depth	Piez. head	NO_3	ID	HU	Depth	Piez. head	NO_3
P237	AHU	n.a.	n.a.	5.16	P277	AHU	12.00	n.a.	n.a.	P317	SHU	8.00	2.41	**75.50**	P357	SHU	7.00	1.20*	**123.50**
P238	SHU	4.00	0.65*	**118.00**	P278	AHU	10.00	7.29	**151.00**	P318	SHU	10.00	2.74	**87.00**	P358	SHU	4.00	n.a.	n.a.
P239	SHU	9.00	0.29	5.14	P279	AHU	25.00	n.a.	n.a.	P319	AHU	11.00	4.91*	10.70	P359	SHU	5.00	3.48	12.50
P240	AHU	4.00	−1.08	38.20	P280	AHU	9.00	7.63	**102.00**	P320	AHU	8.00	5.32	12.00	P360	AHU	8.00	5.29	**72.10**
P241	AHU	60.00	9.03*	15.30	P281	SHU	16.00	3.31*	**84.00**	P321	AHU	8.00	4.45	**73.00**	P361	AHU	56.00	3.08*	38.50
P242	AHU	5.00	21.63*	34.80	P282	SHU	12.00	−0.91	**184.50**	P322	AHU	8.00	1.67	19.00	P362	AHU	10.00	5.58*	28.50
P243	AHU	8.00	n.a.	n.a.	P283	SHU	20.00	3.54*	**200.00**	P323	AHU	5.00	0.70	**52.30**	P363	AHU	8.00	n.a.	**58.70**
P244	AHU	30.00	8.59*	31.80	P284	SHU	12.00	1.58*	37.40	P324	AHU	50.00	−2.10*	**191.50**	P364	AHU	8.00	n.a.	n.a.
P245	AHU	11.00	16.09*	3.37	P285	SHU	30.00	−0.33*	**77.30**	P325	AHU	4.00	−0.02	**66.00**	P365	AHU	5.00	18.19	16.90
P246	AHU	23.00	6.12*	20.10	P286	AHU	50.00	−16.69*	12.50	P326	AHU	8.00	1.87	**119.50**	P366	AHU	30.00	14.71*	**59.60**
P247	SHU	5.00	2.76	**116.00**	P287	AHU	40.00	1.48*	**77.80**	P327	AHU	9.00	3.18	**74.10**	P367	AHU	15.00	7.67*	**72.50**
P248	SHU	35.00	0.42*	**126.00**	P288	AHU	33.00	2.34*	28.20	P328	AHU	10.00	2.30	14.00	P368	AHU	15.00	n.a.	20.00
P249	AHU	35.00	−0.66	49.55	P289	AHU	5.00	0.77	**263.50**	P329	AHU	70.00	n.a.	3.55					
P250	AHU	65.00	−1.07	9.39	P290	AHU	8.00	0.57	**65.40**	P330	AHU	9.00	6.27	13.85					

Hydrogeological units (HU): Alluvial Hydrogeological Unit (AHU). Sandy Hydrogeological Unit (SHU). VHU (Volcanic Hydrogeological Unit); depth is in m; Piezometric head (Piez. head) is in m a.s.l.; nitrate concentration (NO_3) is in mg L^{-1} NO_3. In bold the NO_3 concentrations more than 50 mg L^{-1} NO_3 (threshold value); n.a.: not available.

* dynamic groundwater level

- littoral sediments formed largely by sand and gravel, with some lagoonal silt (Holocene);
- Pleistocene continental deposits, consisting of gravel, with some aeolian sand and alluvial material (Upper Pleistocene).

4.1. Depositional model

In the southern part of the study area (cross-section #3, Fig. 3a), five depositional sequences were recognized. These comprise a typical aggradational stacking produced by a retrogradational step: the base of the sequences consists of an erosional surface covered by terraced alluvial gravels, changing to silty and clayey deposits of lagoonal facies, then sandy deposits of shore face facies, rich in mollusk fossils. These sequences reflect sedimentation in a barrier island–lagoon depositional environment, where eustatic rises have been separated by surface erosion during the subsequent regression phase. During lowstand phases, the base level dropped, so that the deepening river eroded parts of the sediments deposed during the highstand phase, leaving as evidence an erosion surface. The most recent eustatic rise produced the current barrier island–lagoon situation, comprising:

- a sand bar associated with a dune system, represented by the littoral sediments in the Arborea plain;
- a protected lagoon consisting of alluvial clay and loam deposits, represented by the Santa Giusta lagoon in the North and the reclaimed Sassu lagoon in the South;
- an alluvial plain comprising continental deposits and many streams, extending from the Sassu pond eastwards to the Monte Arci volcanic massif.

In the northern part of the Arborea plain, the sedimentary system is complicated by the interference with long-term sediments originating from Tirso River conoids. As is visible in cross-section #8 (Fig. 3b), a system of sand-gravel and discontinuous clay lenses, derived from the Tirso River, is interposed with Pleistocene continental deposits. During the highstand phases, fluvial processes have prevailed in this area. This activity gave rise to a number of sand-gravel bars, and the stream course migrated within the alluvial plain to form a meander. During low water phases, the stream deposited finer sediments as silt and clays, while transporting coarser materials along its bed. Finally, as obtained also with the lowstand phase, the base level dropped, producing the current pattern of deep erosion and channel-straightening. In section, this appears as an irregular stacking of sand-gravel layers in the form of scroll-bars and migrating stream beds, interposed with clay lenses due to the sedimentation of finer materials. Section reconstruction was not possible in the southern portion of the Arborea plain close to the Sassu lagoon, due to the small number of stratigraphic logs available to properly calibrate the VES resistivity logs. However, surface data and characteristics of the two wells present (W8 and W9) (Fig 1b; Table 1) were consistent with a model similar to the one obtained for the northern area. Fluvial conoids, interposed with Pleistocene continental deposits, replaced the lagoonal clays, as well as outcrops in the Sassu lagoon. The direction of continental deposition probably proceeded from west to east. A heteropic contact of facies between littoral sands and continental deposits proceeding from west to east can be assumed. The analysis of the current depositional environment in the Arborea plain suggests a wave-dominated barrier island–lagoon system. The presence of a sand barrier island protected the coastal lagoon in the rear, where the finer sediments carried by streams have been deposited. This is a typical highstand sedimentary model, which results in an increase of accommodation in a coastal plain.

Projecting this model into the recent past assumes that the migration of the system environments was in a direction orthogonal to the current coastline. Provided that the vertical changes in the facies profile correspond through the time at the recording of their longitudinal succession, the expectation is that during a eustatic rise, lagoonal clays would have been overlapped continental alluvial deposits, and in turn littoral sands would have overlapped lagoonal clays. Conversely during a eustatic fall, the coastal plain sediments would have become eroded. The erosion could have affected the lagoonal clays and even the underlying alluvial sediments, which constitute the base of the sedimentary sequence. As a consequence, many of the sequences were reduced to a succession of alluvial sediments at the bottom and lagoonal clays at the top. A highly significant and well understood aspect of this class of depositional model is that the same lithology cannot be deposited simultaneously throughout the depositional profile. As a result, the time line does not coincide with the lithological contacts. Thus, similar sandy bodies observed in two distinct geological logs could not have been deposited during the same period.

4.2. The conceptual hydrogeological model

The conceptual hydrogeological model was built on the base of the geological–depositional system. The hydraulic head survey and the hydrogeological parameters inferred from the stratigraphic well logs and from the literature (i.e. permeability, saturated thickness, specific yield) allow to transform the geological information in hydrogeological features. Three Hydrogeological Units (HU) were identified:

1) *Sandy Hydrogeological Unit* (*SHU*). This unit is represented by a phreatic aquifer hosted in the Holocene littoral sands, cropping out in the Arborea plain and deposited during the most recent marine

transgression. Discontinuous clay lenses of lagoonal origin, which gave rise to perched aquifers (Fig. 3a), characterize the aquifer; therefore, it can be considered locally confined. The aquifer has good porous permeability, with a K value ranging between 10^{-5} and 10^{-6} m s^{-1} (Soddu and Barrocu, 2006). Its geometry has been faithfully reconstructed for the part of the plain lying between the s'Ena Arrubia lagoon to the north, the reclaimed Sassu lagoon to the east and the sea. The aquifer is bounded at its base by a layer of lagoonal clays which reach the surface at ponds (i.e. Sassu Lagoon) lying at an altitude close to 0 m a.s.l., and extend into the sea down to a depth of about 25 m below sea level (Fig. 3a). The thickness of this impermeable boundary is consistently between 25 and 30 m. The sands, which host the aquifer, are 20–25 m deep; depth decreases in an easterly direction to reach zero depth at the lagoons.

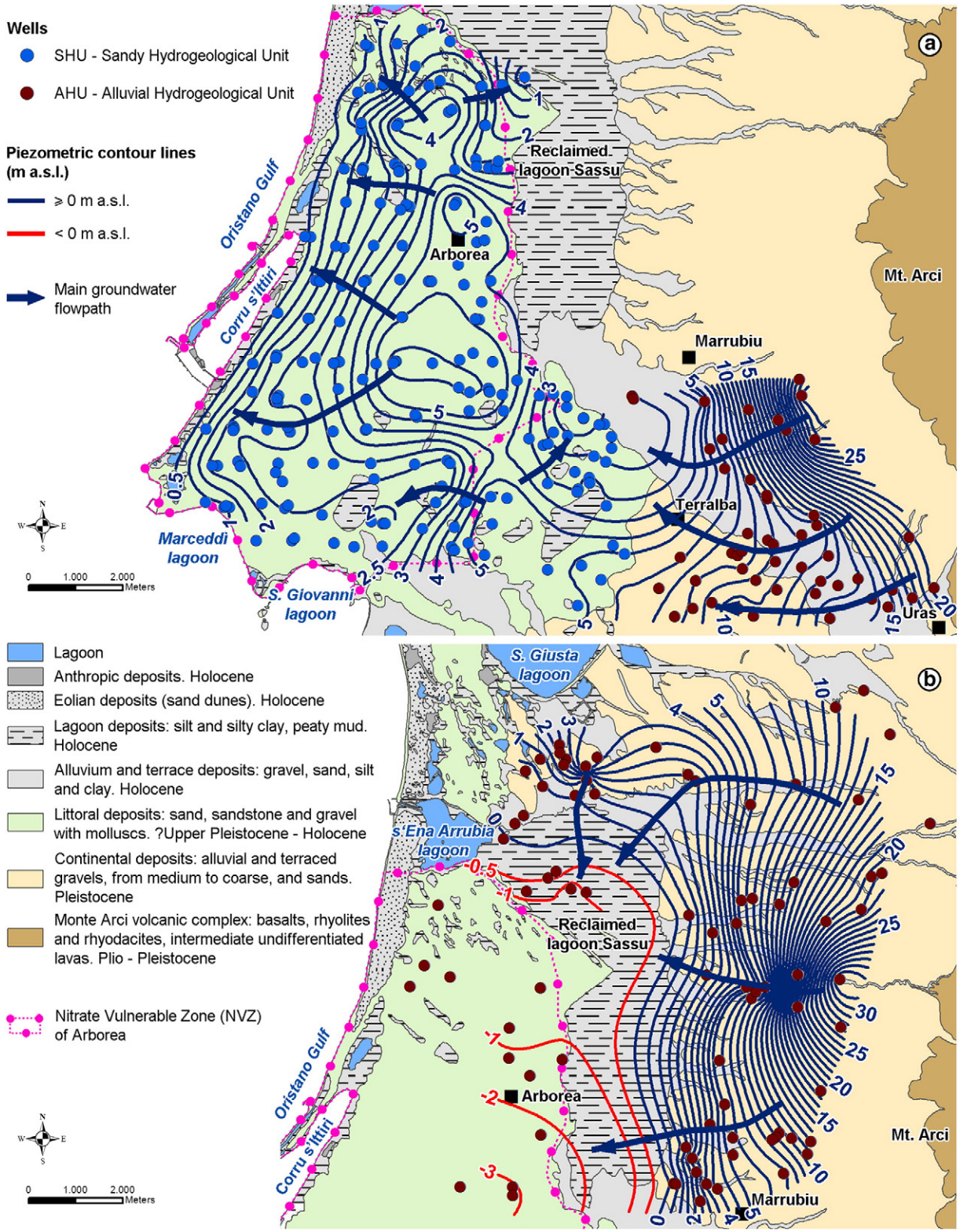

Fig. 5. Piezometric contour lines and main groundwater flow directions in a) the SHU phreatic aquifer; b) the AHU multi-layer aquifer.

Due to the few data available, the aquifer geometry in the southern section of the Arborea plain was reconstructed by the means of the geological–depositional model, which suggested the lack of impermeable boundary (the lagoonal clays) delimiting the bottom of the sandy aquifer. Thus the Holocene sands remain in direct contact with the Pleistocene continental deposits. However, at present it is not possible to determine the depth at which this contact occurs. The implication is that, in this part of the plain, the sandy and alluvial aquifers are in hydraulic communication one to each other.

2) *Alluvial Hydrogeological Unit* (*AHU*). The Pleistocene continental deposits host a multi-layer aquifer. It consists of gravels with some sands or clayey sand outcrops throughout the area surrounding the Arborea plain up to Monte Arci. The maximum thickness of the aquifer can be deduced from the stratigraphic log of well W1 (Pala et al., 1982), which indicates that the depth of the volcanic basement is 300 m below the Quaternary succession. The alluvial aquifer is confined in the Arborea plain because it is bounded at its top by the clay layer, which separates it from the sandy aquifer (SHU). Lagoonal clays represent the impermeable layers, which characterize each depositional sequence (Fig. 3b). In this area, the upper impermeable boundary lies within the range 40–60 m below sea level. Since only a few wells were drilled to a sufficient depth, the aquifer is underexploited (Fig. 3a). This hydrogeological unit also includes good permeability ($K = 10^{-4}$–10^{-5} m s^{-1}) gravelly-sand formations, deposited by fluvial action and intercalated within the continental deposits. The permeability decreases in the sand-clay layers.
3) *Volcanic Hydrogeological Unit* (*VHU*). The aquifer hosted in the volcanic formations cropping out at Monte Arci (Plio-Pleistocene) is composed of basalt, rhyolite and rhyodacite, and shows secondary permeability. The volcanic basement drops rapidly in a westward direction, reaching a sufficient depth to escape access from any well in the plain. As a result, the aquifer is exploited only along a strip of about 2 km from Monte Arci.

Fig. 4 shows the 3D hydrogeological model. This model corroborates the hypothesis that in the southern sector of the Arborea plain the impermeable boundary between the Sandy Hydrogeological Unit (SHU) and the Alluvial Hydrogeological Unit (AHU) is not present, and that the two aquifers are here hydraulically connected. In fact, as shown in the 3D model, the impermeable layer thins out southward, eventually disappearing completely, so that the base of the Sandy Hydrogeological Unit (SHU) coincides with the top of the Alluvial Hydrogeological Unit (AHU).

The volumes of the hydrogeological units have been computed, yielding these results:

- Sandy Hydrogeological Unit (SHU): 1,835,000,000 m^3,
- Confined Alluvial Hydrogeological Unit (AHU): 14,633,000,000 m^3,
- Not confined Alluvial Hydrogeological Unit (AHU): 55,095,000,000 m^3,

4.3. Groundwater circulation and flow paths

The region shows a typical Mediterranean climate, with a mean annual rainfall of 600 mm and a mean annual temperature of 15.7 °C (Lai et al., 2012). Aquifer recharge normally occurs from October to December and from February to April. Groundwater flows were reconstructed on the basis of the piezometric data acquired during the first survey (Table 2) creating a contour line map with groundwater flow directions for aquifers SHU and AHU (Fig. 5a and b). According to the geological and the hydrogeological model, hydraulic communication between the two aquifers under the area to the south of the Sassu lagoon was assumed. Therefore, the piezometric data were considered together for the reconstruction of the piezometric surface in this area (Fig. 5a). In the southern part of the study area, the piezometric contour lines indicate a general flow from east to west, with a gradient which decreases in this direction showing an increase of the trasmissivity. The flow paths suggest a lateral recharge from AHU to SHU.

In the central part of the study area (within the Arborea NVZ), the piezometric surface indicates a zenithal local recharge area for the aquifer hosted in the littoral sands (SHU), with its flow path directed towards the sea. The piezometric contour lines and flow paths related to AHU in the central to northern part of the study area are shown in Fig. 5b. Here, the piezometric surface suggests a general flow direction from east to west, with the exception of the northern sector of the plain, where the direction is more north to south. Around the Sassu lagoon and in the Arborea plain, the piezometric values fall to 3 m below sea level.

Table 3
Summary statistics of NO_3^- concentrations for samples collected in the Arborea plain.

	All samples	AHU	SHU	VHU
	NO_3 mg/L			
n	333	126	190	17
Min	1.58	2.47	1.58	3.24
Max	406	263.5	406	56.5
Median	34.8	37.5	36.1	13.0
Mean	62.0	54.5	70.7	19.4
Stand. dev	67.6	51.8	77.2	15.7
Variance	4570	2682	5955	245
25 prcntil	11.6	12.2	11.4	8.2
75 prcntil	93.5	78.1	105.5	27.9
Skewness	1.8	1.5	1.6	1.3
Kurtosis	3.7	2.2	2.6	0.9
Geom. mean	32.9	32.4	35.9	14.4

4.4. Groundwater NO_3^- concentration

The results of the analytical survey of NO_3^- concentrations are reported in Table 2. The NO_3 concentration ranged between 1.58 and 406 mg L^{-1}. Table 3 reports the summary statistics of nitrates in the identified hydrogeological units. The SHU and AHU waters showed a similar median value, whereas VHU samples showed a lower median concentration (13 mg L^{-1}). In this unit, the 95 percentile of the

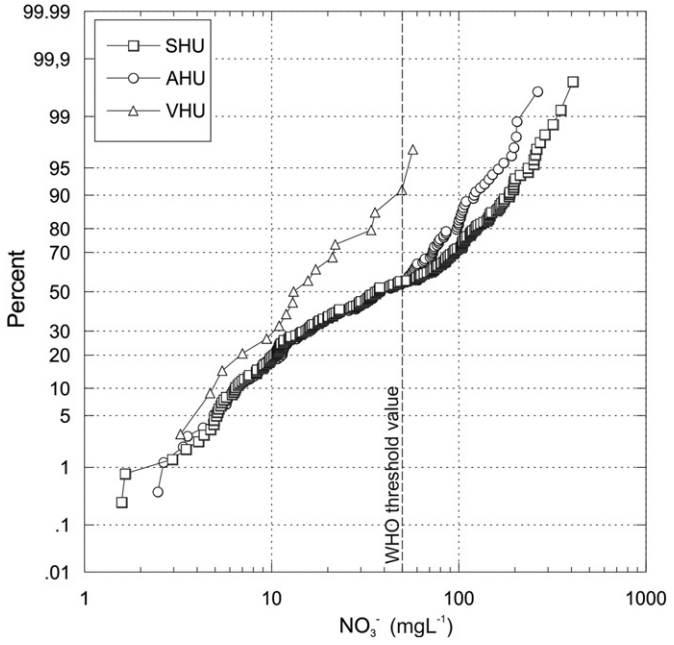

Fig. 6. Cumulate distribution function plot for NO_3^- concentrations in the SHU, AHU and VHU; WHO threshold value of 50 mgL^{-1} is shown.

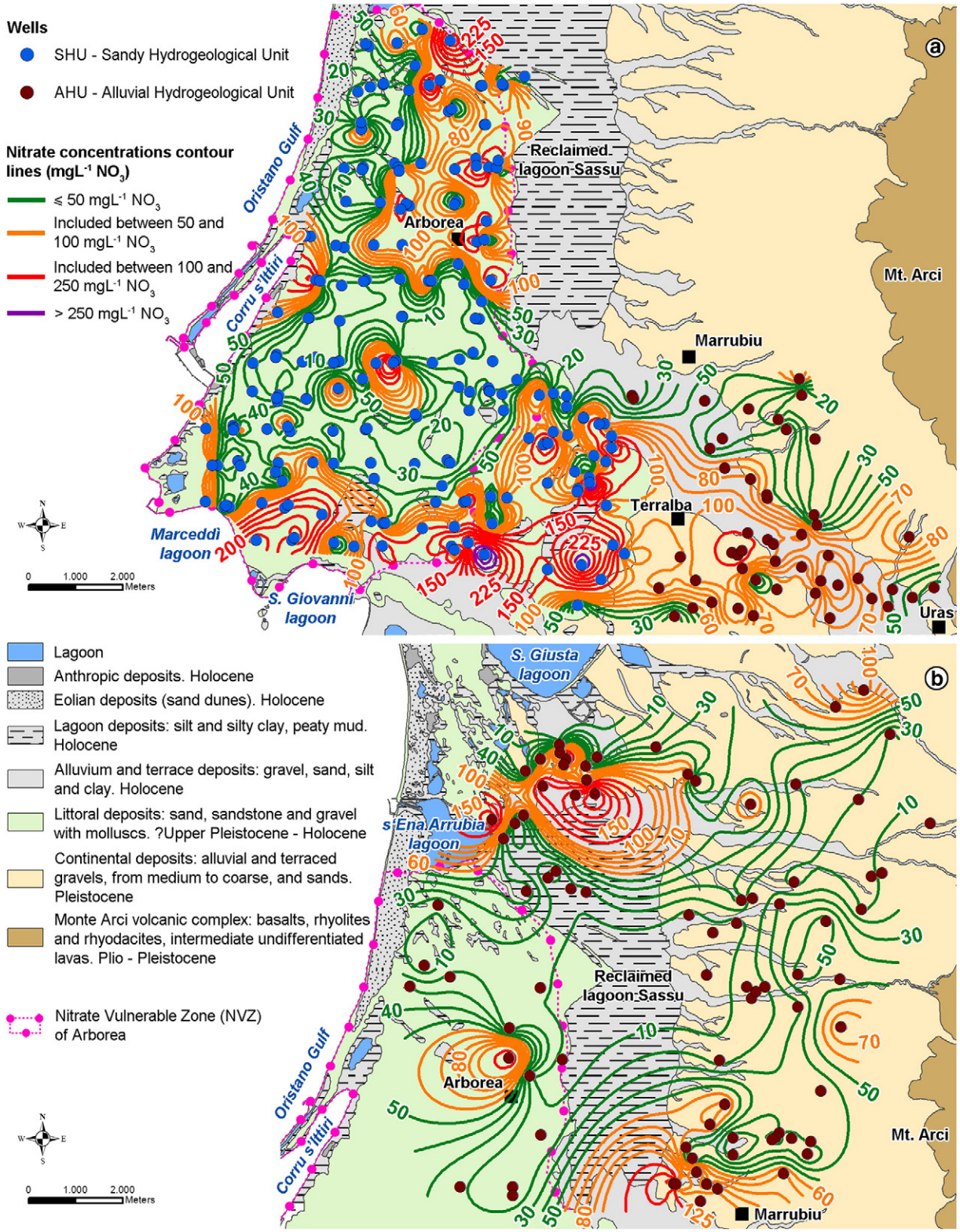

Fig. 7. NO_3^- concentration contour lines in a) the SHU phreatic aquifer; b) the AHU multi-layer aquifer.

population has NO_3^- concentration lower than the WHO threshold value of 50 mg L^{-1} (Fig. 6). By contrast almost the 50% of SHU and AHU waters exceeded the 50 mg L^{-1}; the maximum value of 406 mg L^{-1} was observed in SHU samples.

Concentration contour lines (mg L^{-1} NO_3) in SHU and AHU are respectively reported in Fig. 7a and b. To reconstruct the distribution of NO_3^- concentration in the two aquifers, a similar approach as for the assessment of the groundwater circulation was applied.

In the southern part of the study area, the concentrations were almost uniformly above 50 mg L^{-1} (Fig. 7a). An increasing trend from east to west in the direction of the main groundwater flow prevailed, highlighting a pollution source located outside the Arborea NVZ.

Contributions from NO_3^- sources located within the southern part of the NVZ directly affect SHU. A second highly polluted area was identified in the NE sector of the NVZ. In this zone, the recharge of SHU is local, and there is no contribution from AHU outside of the NVZ. Therefore high NO_3^- value derived from the local anthropogenic activities. In the central portion of the NVZ, sub-threshold concentrations were more common, with some exceptions. The distribution of NO_3^- concentration in AHU is shown in Fig. 7b. This hydrogeological unit is confined below the shallower SHU inside the NVZ, whereas it crops out outside (Figs. 3a, 3 and 4). In this area high concentrations of nitrates were also found, in particular to the north and south-east of the Sassu lagoon. Thus, high concentration of nitrate in the confined AHU may occur both due to improperly installed wells which cause the cross contamination between the two aquifers, and due to solute transport processes from the contaminated recharge areas outside the NVZ.

5. Discussion and conclusions

In this paper a simple but robust methodology to deal with a 3D hydrogeological model of sedimentary coastal aquifers has been elaborated and tested. Sequence stratigraphy, which describes succession through space and time in various depositional systems, has been employed to correlate the sedimentary facies in a reliable and meaningful way.

The analysis of sedimentary processes and depositional environments allowed to properly correlate existing stratigraphic and geophysical data. A similar approach, also employed in reservoir geology and oil prospecting, was successfully applied in similar context in Mediterranean coastal area (Aunay et al., 2006). It allows reconstructing the geometries of the aquifers, which are impossible to define only through the simple correlation between layers identified in the stratigraphic logs. The proposed depositional model of the northern part of the Campidano plain represents an improvement in the state of geological and hydrogeological knowledge regarding the Plio-Quaternary sedimentary succession. The derived hydrogeological conceptual model improves and completes that described by Barroccu et al. (1995, 2004) and Soddu and Barrocu (2006).

These results provide a solid basis for the discrimination of recharge and discharge areas, the groundwater flow directions and the interconnection between aquifers. The two identified sedimentary aquifers (SHU phreatic and AHU-multi layer) were interpreted as separated from each other by a layer of lagoonal clays in the north-central part of the Arborea plain, but hydraulically connected in the southern part of the study area. A preliminary assessment of levels of NO_3^- pollution in the groundwater showed that much of the NO_3^- originates from a part of the plain located outside the Arborea NVZ. Available results show that nitrate pollution in the Arborea area can be attributed mainly to animal manure and secondary to synthetic fertilizers (Pittalis et al., 2014). This finding raises questions regarding the delimitation of the NVZ, which should be enlarged with respect to the monitoring and control activities carried out by the local authorities. Water samples with relatively low nitrate concentrations might be related to denitrification processes (Otero et al., 2009), rather than suggesting a lack of contamination, since land use in this sector is similar to that practiced in other parts of the NVZ. Combining the use of sulfate, boron and nitrogen isotope, Pittalis et al. (2014) observed the occurrence of denitrification and sulfate reduction processes affecting the SHU groundwater of Arborea area both in samples with low and high nitrate concentration. A more detailed study on the hydrogeochemical features of groundwater coupled with isotope techniques and environmental tracers is currently under way to better understand the processes affecting NO_3^- concentration in groundwater.

Built on a good sedimentary model, hydrogeological knowledge must be supplemented by long-time series observation (e.g. hydraulic head, hydrochemistry, and isotope). For future prospects, methodology used in this case could also be applicable to a certain extent to other coastal sedimentary basin.

Finally, the outcomes of the present analyses have provided a firm basis for more detailed studies targeted at groundwater flow modeling, at the identification of recharge areas, and at the characterization of NO_3^- pollution mechanisms in the groundwater. Future research activity should seek to identify the various sources of NO_3^- contamination through more detailed hydrogeochemical and isotope studies.

Acknowledgments

This study was funded by the Autonomous Region of Sardinia in the frame of the Regional Law (LR7/2007) "*Promotion of scientific and technological innovation in Sardinia*" as part of the IDRISK and KNOW projects. The geological modeling was in part funded by a grant to A.F. provided by Foundation Banco di Sardegna (2013.1250). We are grateful to Midland Valley Exploration Ltd. for providing an academic license for the use of Move software.

Authors are also thankful to the EiC Prof. Janusz Wasowski, to two anonymous reviewers and to Prof. Piero Lattanzi for their helpful comments and suggestions to improve the manuscript.

References

Aunay, B., Duvail, C., Giordana, G., Doerfliger, N., Le Strat, P., Montiginoul, M., Pistre, S., 2006. A pluridisciplinary methodology for integrated management of a coastal aquifer. Geological, hydrogeological and economic studies of the Roussillon aquifer (Pyrénées Orientales, France). Vie et Milieu, Life Environ. 56 (4), 275–285.

Barroccu, G., Ghiglieri, G., Uras, G., 1995. Intrusione salina e vulnerabilità degli acquiferi costieri nella piana di Oristano (Sardegna centro-occidentale) [Seawater intrusion and vulnerability of coastal aquifers in the Oristano plain (central and western Sardinia)]. Convegno Gestione Irrigua in Ambiente Mediterraneo, Oristano, Italy. (Technical report, unpublished).

Barroccu, G., Cau, P., Soddu, S., Uras, G., 2004. Predicting groundwater salinity changes in the coastal aquifer of Arborea (central-western Sardinia). Proc. 18th Salt Water Intrusion Meeting (SWIM), Cartagena, Spain.

Best, D.M., Lewis, R.R., 2010. GWVis: a tool for comparative ground-water data visualization. Comput. Geosci. 36, 1436–1442.

Buttau, C., Fanelli, F., Funedda, A., Ibba, A., Loi, A., Pillola, G.L., 2011. Evidence of Quaternary tectonics in SW Sardinia. Rend. Online Soc. Geol. Ital. 15, 11–13.

Canter, L.W., 1997. Nitrate in Groundwater. Lewis, Boca Raton, FL, USA, p. 263 (ISBN 0-87371-569-1).

Carmignani, L., Oggiano, G., Barca, S., Conti, P., Salvadori, I., Eltrudis, A., Funedda, A., Pasci, S., 2001. Geologia della Sardegna. Note illustrative della Carta Geologica della Sardegna a scala 1:200,000 [Geology of Sardinia: notes on the geological map of Sardinia on the scale of 1:200,000]. In: Memorie Descrittive della Carta Geologica d'Italia 60, Istituto Poligrafico e Zecca dello Stato, Rome.

Casmez, 1976. Studio organico delle risorse idriche sotterranee della Sardegna — II fase [Study of groundwater in Sardinia – 2nd phase] Università degli Studi di Sassari, Cassa per il Mezzogiorno (Prog. Cassa 25/96).

Casula, G., Cherchi, A., Montadert, L., Murru, M., 2001. The Cenozoic Graben System of Sardinia (Italy): geodynamic evolution from new seismic and field data. Mar. Pet. Geol. 18, 863–888. http://dx.doi.org/10.1016/S0264-8172(01)00023-X.

Cocco, F., Funedda, A., Patacca, E., Scandone, P., 2013. Plio-Pleistocene extensional tectonics in the Campidano graben (SW Sardinia): preliminary note. Rend. Online Soc. Geol. Ital. 29, 31–34.

Cox, M.E., James, A., Hawke, A., Raiber, M., 2013. Groundwater Visualisation System (GVS): a software framework for integrated display and interrogation of conceptual hydrogeological models, data and time-series animation. J. Hydrol. 491, 56–72.

Dalrymple, R.W., Choi, K., 2007. Morphologic and facies trends through the fluvial–marine transition in tide-dominated depositional systems: a schematic framework for environmental and sequence-stratigraphic interpretation. Earth Sci. Rev. 81, 135–174. http://dx.doi.org/10.1016/j.earscirev.2006.10.002.

Di Maio, R., Fabbrocino, S., Forte, G., Piegari, E., 2014. A three-dimensional hydrogeological–geophysical model of a multi-layered aquifer in the coastal alluvial plain of Sarno River (Southern Italy). Hydrogeol. J. 22, 691–703. http://dx.doi.org/10.1007/s10040-013-1087-8.

Di Salvo, C., Di Luzio, E., Mancini, M., Moscatelli, M., Capelli, G., Cavinato, G.P., Mazza, R., 2012. GIS-based hydrostratigraphic modeling of the city of Rome (Italy): analysis of the geometric relationships between a buried aquifer in the Tiber Valley and the confining hydrostratigraphic complexes. Hydrogeol. J. 20, 1549–1567. http://dx.doi.org/10.1007/s10040-012-0899-2.

Edington, D., Poeter, E., 2006. Stratigraphic control of flow and transport characteristics. Ground Water 44 (6), 826–831. http://dx.doi.org/10.1111/j.1745-6584.2006.00185.x.

Foddis, M.L., Montisci, A., Uras, G., Matzeu, A., Seddaiu, G., Carletti, A., 2012. Prediction of nitrate concentration in groundwater using an Artificial Neural Network (ANN) approach. International Conference on Agricultural Engineering CIGR-AgEng2012, July 8–12, 2012, Valencia.

Ghiglieri, G., Oggiano, G., Fidelibus, D., Barbieri, G., Vernier, A., Tamiru, A., 2009a. Hydrogeology of the Nurra Region, Sardinia (Italy): basement-cover influences on groundwater occurrence and hydrogeochemistry. Hydrogeol. J. 17 (2), 447–466. http://dx.doi.org/10.1007/s10040-008-0369-z.

Ghiglieri, G., Barbieri, G., Vernier, A., Carletti, A., Demurtas, N., Pinna, R., Pittalis, D., 2009b. Aquifers potential risk pollution by agricultural nitrates: Nurra region (NW Sardinia, Italy). J. Hydrol. 379, 339–350. http://dx.doi.org/10.1016/j.jhydrol.2009.10.020.

Ghiglieri, G., Carletti, A., Pittalis, D., 2012. Analysis of salinization processes in the coastal carbonate aquifer of Porto Torres (NW Sardinia, Italy). J. Hydrol. 432–433 (11), 43–51. http://dx.doi.org/10.1016/j.jhydrol.2012.02.016.

Giola, P., Basso, B., Pruneddu, G., Giunta, F., Jones, J.W., 2012. Impact of manure and slurry applications on soil nitrate in a maize–triticale rotation: field study and long term simulation analysis. Eur. J. Agron. 38, 43–53. http://dx.doi.org/10.1016/j.eja.2011.12.001.

Irace, A., Clemente, P., Piana, F., De Luca, D.A., Polino, R., Violanti, D., Mosca, P., Trenkwalder, S., Natalicchio, M., Ossella, L., Governa, M., Petricig, M., 2010. Hydrostratigraphy of the late Messinian–Quaternary basins in southern Piedmont (northwestern Italy). Memorie Descrittive Carta Geologica d'Italia XC, pp. 133–152.

Jones, R.R., McCaffrey, K.J.W., Clegg, P., Wilson, R.W., Holliman, N.S., Holdsworth, R.E., Imber, J., Waggott, S., 2009. Integration of regional to outcrop digital data: 3D visualisation of multi-scale geological models. Comput. Geosci. 35, 4–18.

Koefoed, O., 1972. A note on the linear filter method of interpreting resistivity sounding data. Geophys. Prospect. 20, 403–405.

Koefoed, O., 1979. Geosounding Principles, 1: Resistivity Sounding Measurements. Elsevier Science Publ. Co. Inc.

Lai, R., Seddaiu, G., Gennaro, L., Roggero, P.P., 2012. Effects of nitrogen fertilizer sources and temperature on soil CO_2 efflux in Italian ryegrass crop under Mediterranean conditions. Ital. J. Agron. 7, e27.

Lecca, L., Carboni, S., 2007. The Tyrrhenian section of San Giovanni di Sinis (Sardinia): stratigraphic record of an irregular single high stand. Riv. Ital. Paleontol. Stratigr. 113 (3), 509–523.

Lemon, A.M., Jones, N.L., 2003. Building solid models from boreholes and user-defined cross-sections. Comput. Geosci. 29 (5), 547–555.

O'Neill, D.J., Merrick, N.P., 1984. A digital linear filter for resistivity sounding with a generalized electrode array. Geophys. Prospect. 32, 105–123.

Oggiano, G., Funedda, A., Carmignani, L., Pasci, S., 2009. The Sardinia–Corsica microplate and its role in the Northern Apennine Geodynamics: new insights from the Tertiary intraplate strike-slip tectonics of Sardinia. Ital. J. Geosci. 128 (2), 527–541. http://dx.doi.org/10.3301/IGJ.2009.2.527.

Otero, N., Torrentó, C., Soler, A., Menciò, A., Mas-Pla, J., 2009. Monitoring groundwater nitrate attenuation in a regional system coupling hydrogeology with multi-isotopic methods: the case of Plana de Vic (Osona, Spain). Agric. Ecosyst. Environ. 133 (1–2), 103–113.

Pala, A., Pecorini, G., Porcu, A., Serra, S., 1982. Geologia e idrogeologia del Campidano (Geology and hydrogeology of Campidano). Ricerche Geotermiche in Sardegna, CNR-PFE-SPEG-RF10, CNR-Pisa, pp. 87–103.

Pittalis, D., Biddau, R., Carletti, A., Demurtas, C., Roggero, P.P., Ghiglieri, G., Cidu, R., 2014. A multi-isotopic approach to evaluate origin and fate of nitrate in groundwater hosted in a NVZ Sardinian area. Flowpath 2014, National Meeting on Hydrogeology, IAH Italian Chapter, Viterbo, June, 18–20, Abstract Volume, pp. 74–75 http://dx.doi.org/10.13140/2.1.1423.5840.

Pomesano-Cherchi, A., 1971. Studio stratigrafico e micro paleontologico del pozzo Oristano 1 (Sardegna) (Stratigraphical and micropaleontological study of the well Oristano 1 (Sardinia)). Mem. Soc. Geol. Ital. 10, 1–16.

Raiber, M., White, P.A., Daughney, C.J., Tschritter, C., Davidson, P., Bainbridge, S.E., 2012. Three-dimensional geological modelling and multivariate statistical analysis of water chemistry data to analyse and visualise aquifer structure and groundwater composition in the Wairau Plain. Marlborough District. New Zealand. J. Hydrol. 436-437, 13–34. http://dx.doi.org/10.1016/j.jhydrol.2012.01.045.

Sacco, D., Offi, M., De Maio, M., Grignani, C., 2007. Groundwater nitrate contamination risk assessment: a comparison of parametric systems and simulation modelling. Am. J. Environ. Sci. 3 (3), 117–125 (ISSN: 1553-345).

Smirnoff, A., Boisvert, E., Paradis, S.J., 2008. Support vector machine for 3D modeling from sparse geological information of various origins. Comput. Geosci. 34 (2), 127–143.

Soddu, S., Barrocu, G., 2006. Contaminazione salina degli acquiferi nell'area della Bonifica di Arborea (Sardegna centro-occidentale) (Aquifers salinization in the Arborea area (central and western Sardinia)). Rivista IGEA — Ingegneria e Geologia degli Acquiferi Vol. 21, pp. 103–112.

Steinich, B., Escolero, O., Marín, L.E., 1998. Salt-water intrusion and nitrate contamination in the Valley of Hermosillo and El Sahuaral coastal aquifers, Sonora, Mexico. Hydrogeol. J. 6, 518–526.

Tremblay, T., Nastev, M., Lamothe, M., 2010. Grid-based hydrostratigraphic 3D modelling of the Quaternary sequence in the Chateauguay River Watershed, Quebec. Can. Water Resour. J. 35 (4), 377–398.

WHO, 2003. Nitrate and Nitrite in Drinking-Water. Background Document for Preparation of WHO Guidelines for Drinking Water Quality. World Health Organization, Geneva (WHO/SDE/WSH/03.04/56).

Wu, Q., Xu, H., Zou, X., 2005. An effective method for 3D geological modeling with multi-source data integration. Comput. Geosci. 31, 35–43.

Wycisk, P., Hubert, T., Gossel, W., Neumann, C., 2009. High-resolution 3D spatial modeling of complex geological structures for an environmental risk assessment of abundant mining and industrial megasites. Comput. Geosci. 35 (1), 165–182.

Zalidis, G., Stamatiadis, S., Takavakoglou, V., Eskridge, K., Misopolinos, N., 2002. Impacts of agricultural practices on soil and water quality in the Mediterranean region and proposed assessment methodology. Agric. Ecosyst. Environ. 88, 137–146.